Available online at www.sciencedirect.com
SCIENCE DIRECT®
International Journal of Solids and Structures 42 (2005) 1743–1758
INTERNATIONAL JOURNAL OF SOLIDS and STRUCTURES
www.elsevier.com/locate/ijsolstr

Defect identification in laminated composite structures by BEM from incomplete static data

Guillermo Rus [a,b], Sang-Youl Lee [a,*,1], Rafael Gallego [b]

[a] Department of Civil and Environmental Engineering, Massachusetts Institute of Technology, Cambridge, MA 02139, USA
[b] Department of Structural Mechanics, University of Granada, Politécnico de Fuentenueva, 18071 Granada, Spain

Received 27 December 2003; received in revised form 26 July 2004
Available online 18 September 2004

Abstract

This work examines the identification of defects in anisotropic laminated composite structures using the boundary element method (BEM) from incomplete static response data including noise effects. The main objective in this paper is to anticipate effects of layup sequences and sensitivity of a measurement system of two-dimensional structures made of composite materials for detecting defects. It is a key goal to create understanding on the influence of the monitorization of advanced structures into their design. The identifiability is studied in terms of layup, measurement and loading design by using boundary element modeling. The concept of identifiability is based on the existing inversion strategy, which consists of the minimization of a cost functional with the possibility of taking into account the entire measurement-specimen system, and therefore interpreting quantitatively the measurements. In this article, after verifying that the boundary element model is in good agreement with numerical results reported by other investigators, the effect of noise in the measurements on the identifiability is studied with respect to different design parameters of laminated composites using a wide set of numerical examples.
© 2004 Elsevier Ltd. All rights reserved.

Keywords: Identifiability; Probability of detection (POD); BEM; Laminated composites; Non-destructive evaluation (NDE); Inverse problems (IP); Noise effects

1. Introduction

With the advancement of technology in fiber-reinforced composite materials, the applicability of composites to structural members has been increased significantly due to their merits such as low density, high

* Corresponding author. Tel.: +82 24005200; fax: +82 24009134.
E-mail addresses: leesy@mit.edu, leesangyoul@hanmail.net (S.-Y. Lee).
[1] Present address: SQ Engineering Co., 160-11, Karak-Dong, SongPa-Gu, Seoul 138-160, South Korea

0020-7683/$ - see front matter © 2004 Elsevier Ltd. All rights reserved.
doi:10.1016/j.ijsolstr.2004.07.028

stiffnesses and high strength. Consequently, the need for safe monitorization and predictive non-destructive evaluation (NDE) and other inverse problems (IP) in such sensitive and expensive structures is constantly increasing.

Structural analysis of anisotropic composite materials using BEM has been studied previously by a number of investigators. The first application of the BEM for composite materials is due to Cruse and Swedlow (1971). Later, the formulation was extended to two-dimensional crack problems by Snyder and Cruse (1975) and a general three-dimensional problem was presented by Wilson and Cruse (1978). On the other hand, the first extension to two-dimensional elastodynamic in the time domain was developed by Wang et al. (1996). Other applications of BEM for adhesively bonded patches can be found in Young and Rooke (1992). Recently, Lingyun and Daniel (1998) analyzed two-dimensional micro-mechanical behaviors of composite materials using BEM. A new boundary element formulation for the mechanically fastened composite patch was developed by Widagdo and Aliabadi (2001). Theses works, based on forward approaches, deal with static or dynamic responses of the structural system from external conditions such as loading.

For the inverse approach, a recent survey investigated by Achenbach (2000) addresses the importance of coupling the concept of probability of detection (POD) and the measurement model on quantitative NDE. This is a representation of the probability that a given measurement system will be able to detect a specific defect in a given material or structure. This area of research has been merely empirical until very recently. Ogilvy (1993) presented a model that relates the probability of detection and of false indication in a conventional pulse-echo detection of well-oriented planar defects with ultrasonics. Rajesh et al. (1992) studied the POD by running a probabilistic FEM model for eddy current NDE. In this paper, the concept of identifiability using the POD is applied to identify defects.

For the present approach to quantitative defect identification, in opposition to standard imaging techniques, the output data is reduced from the classical being the complete bitmap of the image to a reduced set of parameters that gives an univocal description and characterization of the defect. This procedure, called parametrization, is based on assimilating the defect to a simple geometrical entity, defined by the reduced set of parameters P, which are the unknowns of the inverse problem. This reduction is appropriated when the noise in imaging is too big, and the compromise of the assumption of a simplified geometry of the defect is acceptable. The use of this parametrization has been used under different names in conjunction with boundary oriented numerical methods. The first attempt performed by Bezerra and Saigal (1993), Mellings and Aliabadi (1995) and Yao and Gong (1994) for 2D elastostatic isotropic plates. Burczyński (1993) made an extensive research on the development of the sensitivity analysis by using the BEM. The computation of the sensitivity has been studied using direct derivation by Aithal and Saigal (1995), Tanaka and Masuda (1989), Gallego and Suárez (1999) and Rus and Gallego (2002a,b) using the adjoint variable method (Burczyński, 1995; Bonnet, 1995; Bonnet, 1999) and other techniques (Kane and Guru Prasad, 1993; Nishimura, 1997). Other non-gradient based methods such as genetic algorithms or neural networks have also been used (Stavroulakis and Antes, 1998; Stavroulakis, 2001; Lee and Wooh, in press; Boström and Wirdelius, 1995; Wirdelius, 1994). Calmon et al. (1998) also used approximate ultrasonic models in the framework of an optimization algorithm. However, all these works are limited, in that they can analyze only the structural members made of isotropic materials.

In this paper, the previous concepts are extended from isotropic materials to anisotropic laminated composite materials. The main objective in this paper is to find how the design of the composite material affects and how sensitive a measurement system is to the presence and evaluation of defects. The latter concept may be referred as *identifiability*. In other words, this paper intends to establish criteria on the influence of the monitorization of defects into the design of composites. The word identifiability of parameters is used within the finite element method in a completely different sense by Linderholt and Abrahamsson (2003). They emphasize that the correct way of reducing noise is re-parametrizing in order to avoid parameters that lack identifiability. They also propose a method based on singular value decomposition (SVD) for simple parametrizations. In this article, the basic principle of the identifiability is twofold. First, the measured dis-

turbance due to the presence of a defect should be maximized, and second, its magnitude should stand out of that of the noise. In particular, the input data for the problem in this paper is given in terms of the geometrical and mechanical characterization of the specimen to be evaluated and in terms of a set of measurements of its response to a mechanical excitation. For the solution of the inverse problem we choose procedures based on the minimization of the discrepancy between measured and predicted response (Gallego and Suárez, 1999; Rus and Gallego, 2000; Suárez, 1998).

2. Formulation of anisotropic multilayer composites

For completeness, the relevant formulas in the boundary element analysis of two-dimensional laminated composite bodies are reviewed below (Lee et al., 1997). Fig. 1 shows the structural and material axes of a two-dimensional anisotropic body. From Fig. 1, the transformed tensor σ_{ij} of the plane stresses σ_{pq} between the structural and material axes is

$$\sigma_{ij} = l_{ip}\sigma_{pq}l_{qj} \quad (i,j,p,q = 1,2,6), \tag{1}$$

where matrix l_{ij} is the transformation matrix. The relationship between the displacement vector u_i and the linear strain tensor ϵ_{ij} is given through the compatibility equation,

$$\epsilon_{ij} = \frac{1}{2}(u_{i,j} + u_{j,i}). \tag{2}$$

In the generalized Hooke's law, a two-dimensional anisotropic composite material stiffness C_{ij} and flexibility a_{ij} can be expressed in the following convenient form using the single-subscript notation for stress and strain components and the double-subscript notation for elastic constants:

$$\sigma_i = C_{ij}\epsilon_j, \quad \epsilon_i = a_{ij}\sigma_j \quad (i,j = 1,2,6). \tag{3}$$

Following the notation of Lekhnitskii (1981), the flexibility matrix $[a_{ij}]$ for orthotropic material in the material axes in terms of engineering constants can be written as

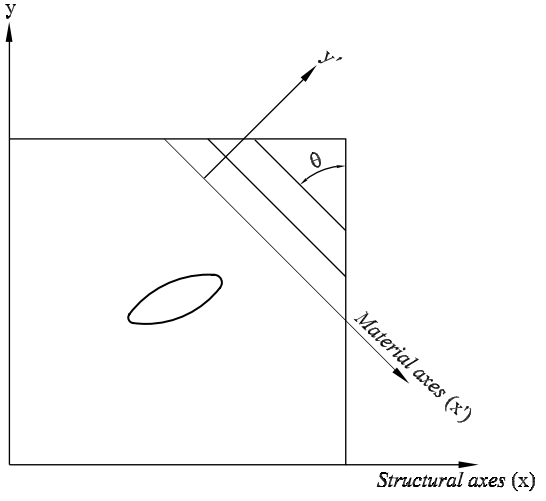

Fig. 1. Structural and material axes.

$$[a_{ij}] = \begin{bmatrix} 1/E_1 & -v_{21}/E_2 & 0 \\ -v_{12}/E_1 & 1/E_2 & 0 \\ 0 & 0 & 1/G_{12} \end{bmatrix}, \tag{4}$$

where E_i, v_{ij}, and G_{12} denote elastic moduli, Poisson's ratios, and shear modulus, respectively. Combining Eqs. (1)–(3) by using transformation from the material coordinate system, the stress-displacement relationship follows as

$$\tilde{\sigma}_i = l_{ij}\sigma_j = l_{ij}C_{ij}\epsilon_j = l_{ij}C_{ij}l_{ij}^T\tilde{\epsilon}_j = \overline{C}_{ij}\tilde{\epsilon}_j, \tag{5}$$

$$\tilde{\epsilon}_i = \bar{a}_{ij}\tilde{\sigma}_j, \tag{6}$$

In order to analyze a multilayered anisotropic material we model the combination of single layers as follows. We proceed deriving the constitutive equations that relate the force resultants to the strains of a laminate. Eq. (6) holds for the kth lamina in the problem coordinates. The integration of stresses through the laminate z-thickness requires laminawise integration. Hence, the force resultants N_i are given by

$$N_i = \sum_{k=1}^{n} \int_{z_k}^{z_{k+1}} \tilde{\sigma}_i \, \mathrm{d}z = \sum_{k=1}^{n} \int_{z_k}^{z_{k+1}} \overline{C}_{ij}\tilde{\epsilon}_j = \tilde{C}_{ij}\tilde{\epsilon}_j, \tag{7}$$

$$\tilde{\epsilon}_i = \bar{A}_{ij}N_j, \tag{8}$$

where n is the number of layers.

This model is taken into account into the BEM through the fundamental solution derived from it. For the two-dimensional analysis of a generally anisotropic medium, the fundamental solutions are given by the following closed forms. u_j^i and q_j^i are the jth components of the displacement and traction at the observation point due to a singular load at a distance z towards direction i.

$$u_i^j = 2\mathrm{Re}[A_{i1}B_{j1}\ln z_1 + A_{i2}B_{j2}\ln z_2] \quad (i,j=1,2), \tag{9}$$

$$q_i^j = 2\mathrm{Re}\left[\frac{A_{i1}\overline{C}_{j1}}{z_1}(\mu_1 n_1 - n_2) + \frac{A_{i2}\overline{C}_{j2}}{z_2}(\mu_2 n_1 - n_2)\right] \quad (i,j=1,2), \tag{10}$$

where μ_k are the complex roots of the characteristic polynomial,

$$a_{11}\mu^4 - 2a_{16}\mu^3 + (a_{12}+a_{66})\mu^2 - 2a_{16}\mu + a_{22} = 0, \tag{11}$$

and the complex constants B_{kl} in Eq. (10) are given as follows:

$$\begin{pmatrix} B_{1l} \\ B_{2l} \end{pmatrix} = \begin{pmatrix} a_{11}\mu_l^2 + a_{12} - a_{16}\mu_l \\ a_{12}\mu_l + a_{22}/\mu_l - a_{26} \end{pmatrix}, \tag{12}$$

and $C_{1k} = \mu_k$, $C_{2k} = -1$, and A_{kl} are the complex roots of

$$\begin{pmatrix} 1 & -1 & 1 & -1 \\ \mu_1 & -\tilde{\mu}_1 & \mu_2 & -\tilde{\mu}_2 \\ B_{11} & -\tilde{B}_{11} & B_{12} & -\tilde{B}_{12} \\ B_{21} & -\tilde{B}_{21} & B_{22} & -\tilde{B}_{22} \end{pmatrix} \begin{pmatrix} A_{k1} \\ \tilde{A}_{k1} \\ A_{k2} \\ \tilde{A}_{k2} \end{pmatrix} = \begin{pmatrix} \frac{\delta_{k2}}{2\pi i} \\ \frac{\delta_{k1}}{2\pi i} \\ 0 \\ 0 \end{pmatrix}. \tag{13}$$

3. Boundary element method

In some class of IP, the use of the BEM provides clear advantages in comparison with the finite element method and others. First, it does not require a remesh of the domain of the body at each iteration. This reduces both the computational effort and eliminates small but important perturbations due to changes of the mesh. Second, the application of these methods to real problems may require many iterations, as well as high precision in the intermediate solutions, so the use of finite elements would be very expensive.

The integral equation we use for the BEM is one that directly relates u_i and q_i. In the equilibrium equation ($\sigma_{ij,j} + b_i = 0$), the principle of the inner product or weak formulation is given as

$$\int_\Omega (\sigma_{ij,j} + b_i) w_i \, \mathrm{d}\Omega = 0, \tag{14}$$

where w_i is a weight function. If we choose the previously obtained fundamental solution u^i_k as the kernel function, and integrate it by parts twice the first component, we obtain Betti's reciprocity theorem:

$$\int_\Omega \sigma^i_{jk,j} u_k \, \mathrm{d}\Omega + \int_\Omega b_i u^i_k \, \mathrm{d}\Omega = -\int_\Gamma \sigma_{jk} n_j u^i_k \, \mathrm{d}\Gamma + \int_\Gamma \sigma^i_{jk} n_j u_k \, \mathrm{d}\Gamma. \tag{15}$$

The reason for choosing a singular fundamental solution is that the identity $\sigma^i_{jk,j} + \delta(\mathbf{y} - \mathbf{x}) e_i = 0$ (where $\mathbf{y}$ is the pole and $\mathbf{x}$ is the observation point), converts the first domain integral into a single-point value (the kernel is zero-valued everywhere except at the pole), giving

$$-u_i(\mathbf{y}) + \int_\Omega b_k u^i_k \, \mathrm{d}\Omega = -\int_\Gamma \sigma_{jk} n_j u^i_k \, \mathrm{d}\Gamma + \int_\Gamma \sigma^i_{jk} n_j u_k \, \mathrm{d}\Gamma. \tag{16}$$

Neglecting body forces in Eq. (16), the integral equation at the boundary is obtained

$$u_i(\mathbf{y}) = \int_\Gamma (q_k u^i_k - q^i_k u_k) \, \mathrm{d}\Gamma. \tag{17}$$

Eq. (17) can be turned into a boundary integral equation if we take the pole $\mathbf{x_i}$ to the boundary. In this case the integrals can turn singular. After a careful limiting process, Eq. (17) turns into:

$$c^i_k(\mathbf{y}) u_k(\mathbf{y}) + \int_\Gamma \left[q^i_k(\mathbf{x};\mathbf{y}) u_k(\mathbf{x}) - u^i_k(\mathbf{x};\mathbf{y}) q_k(\mathbf{x}) \right] \mathrm{d}\Gamma(\mathbf{x}) = 0, \tag{18}$$

where the integrals have the sense of Cauchy Principal Value, which has to be evaluated numerically using so-called regularization techniques (Domínguez, 1993; Rus and Gallego, 2002a,b). Any of the equations above are valid for a continuum problem. We express the continuum in terms of discrete values by

$$x_k = \sum \phi_j x^k_j \quad u_k = \sum \phi_j u^k_j \quad q_k = \sum \phi_j q^k_j. \tag{19}$$

A determined system of equations is constructed writing the boundary integral equation once for every collocation point and direction. The system is then reorganized so as to include all unknown displacements u_i and tractions q_i in vector $\mathbf{v}$, according to the boundary conditions.

$$\mathbf{Hu} = \mathbf{Gq} \Rightarrow \mathbf{Av} = \mathbf{b}. \tag{20}$$

4. Identifiability and inverse problem

The concept of identifiability should be defined within the context of the complete solution of an IP. It represents the probability of a defect to stand out of the noise of the measurements with a minimum deviation.

A BEM model is used in an IP solution strategy based on minimization of discrepancy. First, the specimen is loaded with a specific case in order to provoke a clearly measurable deformation. Then, the static deformed shape is measured at several points and directions, each of them giving a magnitude called measurement. The detection is then based on the minimization of a residual R between the amplitudes at the receiver transducers v^m and the computed predictions of them by this method $v^c(P_g)$.

$$R = v^m - v^c(P_g), \tag{21}$$

where $v^c(P_g)$ is a function of the parameters P_g that describe the flaws. The significant idea of the IP solution is the optimization of a cost functional with respect to the parameters P_g. The cost functional in this paper is defined in a least squares sense. The residual function can be written as

$$L = \frac{1}{2} R^T R. \tag{22}$$

Instead of minimizing L, we define the cost function Ψ as a value to be maximized

$$\Psi = -\log(L + \epsilon), \tag{23}$$

The reason for this choice is that it is better suited and gives better results when applied to certain optimization techniques such as genetic algorithms (Gallego and Rus, 2001).

For the parametrization scheme we make use of a modified field $\tilde{x}_i$ of the original geometry x_i (Rus and Gallego, 2002a,b), expressing the change of position of each material point. For our particular case, we have chosen a very simple non-linear parametrization capable of representing flaws assuming any elliptical shape, size and orientation (Table 1 shows each parameter of the vector P_g):

$$\tilde{x}_i(P_g) = \begin{bmatrix} p_1 + (p_3 \cos p_5 - p_4 \sin p_5) \\ p_2 + (p_3 \sin p_5 + p_4 \cos p_5) \end{bmatrix}. \tag{24}$$

To study the identifiability, from the expansion of the residual vector R in terms of the parameters P_g, Eq. (21) can be rewritten as

$$R = \frac{\mathrm{d}R}{\mathrm{d}P_g}(P_g - P_g^r) + \mathrm{HOT}, \tag{25}$$

where P_g^r means the measured parameters and HOT stands for higher order terms. The residual functional L in Eq. (22) leads to the expansion by using Eq. (25) as following:

$$L(P_g) = L(P_g^r) + \frac{\mathrm{d}L(P_g^r)}{\mathrm{d}P_g}(P_g - P_g^r) + \frac{1}{2}\frac{\mathrm{d}^2 L(P_g^r)}{\mathrm{d}P_g^2}(P_g - P_g^r)^2 + \mathrm{HOT} \approx \frac{1}{2}\frac{\mathrm{d}^2 L(P_g^r)}{\mathrm{d}P_g^2}(P_g - P_g^r)^2 \tag{26}$$

in the vicinity of the real defect. By using Eq. (26), the cost functional Ψ in Eq. (23) is then approximated to

$$\Psi \approx -\log\left(\frac{1}{2}\frac{\mathrm{d}^2 L(P_g^r)}{\mathrm{d}P_g^2}(P_g - P_g^r)^2 + \epsilon\right) \approx -\log\left(\frac{(P_g - P_g^r)^2}{2}\right) - \log\left(\frac{\mathrm{d}^2 L(P_g^r)}{\mathrm{d}P_g^2}\right) \tag{27}$$

Table 1
Definition of the parameter vector P_g

Parameter	Definition
x_1^{cg}	Horizontal coordinate of the centroid of the flaw
x_2^{cg}	Vertical coordinate of the centroid of the flaw
a	Horizontal size
b	Vertical size
α	Angle of rotation (radians)

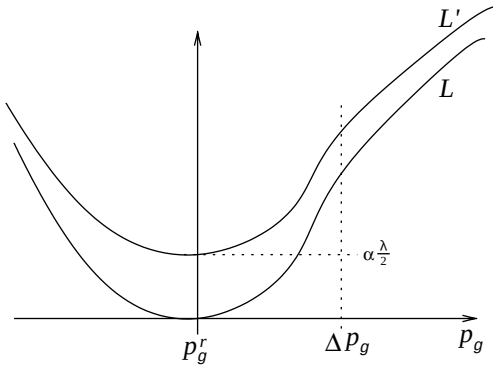

Fig. 2. Representation of concepts of parameters and residual functionals for identifiability.

in which the second term can be related to the level of noise in the following way.

If the residual vector is assumed to contain incomplete data such as a noise terms proceeding from the measurements or whatever other source, R in Eq. (25) can be redefined to R', adding a prime ($'$) that denotes the presence of noise, as

$$R' = R + \alpha n, \tag{28}$$

where n is a gaussian stochastic process with zero mean and unity variance, and α defines the magnitude of the noise. In this case, the residual functional is also modified to

$$L' = L + \alpha\sqrt{2\lambda L} + \alpha\frac{\lambda}{2}, \tag{29}$$

where λ is the length of the residual vector. For a given probability, the highest expected value of the residual functional L at the position of the real defect ($P_g = P_g^r$) will be $L' = \alpha\frac{\lambda}{2}$, which can be compared to its average value ($n = 0$ or $L' = L$), as shown in Fig. 2, for a required range of values of the identification parameter $P_g \pm \Delta P_g$ to find the following:

$$L' = L = \frac{1}{2}\frac{\mathrm{d}^2 L(P_g^r)}{\mathrm{d}P_g^2}\Delta P_g^2 = \alpha\frac{N}{2} \Rightarrow \log\left(\frac{\mathrm{d}^2 L(P_g^r)}{\mathrm{d}P_g^2}\right) = \log\left(\frac{\alpha N}{\Delta P_g^2}\right). \tag{30}$$

Two key aspects have been concluded here to quantitatively improve the identifiability.

First, the larger the noise for the required range of identifiability ratio, the higher the term $\left[-\log\left(\frac{\mathrm{d}^2 L(P_g^r)}{\mathrm{d}P_g^2}\right)\right]$ needs to be. In other words, higher values of Ψ in the vicinity of the defect means higher identifiability, in an additive sense. The second one is that the wider the peak with the defect, the easier it is to find it for a search algorithm especially for zero-order methods, genetic algorithms, and gradient based ones. These conclusions are the key to interpret the cost functional graphics shown in the following sections, and extract conclusions about the identifiability.

5. Numerical results

The methodology described above to find the position and size of defects is implemented an tested numerically to assess its functionality. Furthermore, the limitations of this methodology are sought by a parametric study of the noise effects for various load cases, angle and layer layup, and value of the

parameters. The concept of identifiability is demonstrated in the results in relationship with the level of noise.

5.1. Methodology and validation of results

In this paper, two models which are combinations of two specimen shapes under two different load cases each are used as shown in Fig. 3. They consist of rectangular plates of layered composite materials under aligned loads, which makes them 2D problems. Since the defects have close to null stiffness properties, they are correctly modeled as elliptical holes of a variable angle, size and position, which are to be determined.

The material is a layered composite with a variable number of layers and a specific sequence of cross or angle ply. The properties of composite materials in this study are listed in Table 2. Due to the use of several parameters, the procedure will be to keep one parameter fixed while moving the rest. 40 quadratic boundary elements integrated using 8-point gauss quadrature each are used. The unknowns and collocation points are placed according to the scheme of conforming elements (Domínguez, 1993). In addition, an adimensionalization scheme for all the magnitudes toward unity values has been used. It works introducing a new system of magnitudes and establishing the necessary correspondence with the input system (Rus, 2001). The motivation is to overcome numerical instabilities of the inversion procedure introduced by Rus and Gallego (2002a,b).

The boundary element formulation described earlier is now implemented to compare the results in the isotropic case with unity Young modulus and 0.3 Poisson ratio computed by Rus and Gallego (2002a,b). The problem is depicted as well as the points from which the comparison data have been taken are represented in Fig. 4 and Table 3. The values in Table 3 are appropriately coincident (errors within 3.5% for the chosen 40-elements discretization), giving enough confidence on the boundary element code. However, the correct convergence will be checked as the number of elements is increased. A convergence check of the

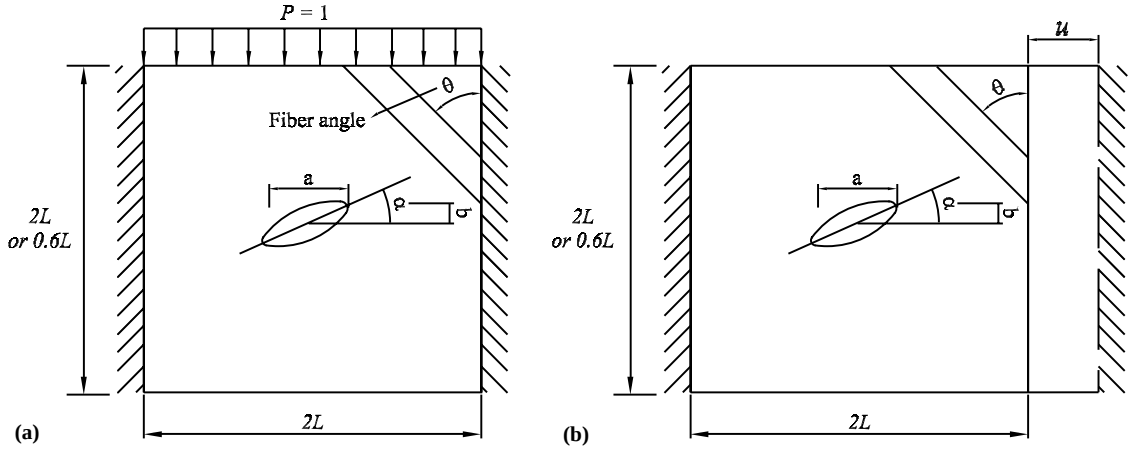

Fig. 3. Description of the models: (a) loadcase 1 and (b) loadcase 2.

Table 2
Properties of the materials used in this study

Materials	E_1 (N/m^2)	E_2 (N/m^2)	G_{12} (N/m^2)	v_{12}
Graphite-epoxy (AS/3501)	137.90×10^9	8.9635×10^9	7.1019×10^9	0.30
Glass-epoxy	53.781×10^9	17.927×10^9	8.9635×10^9	0.25

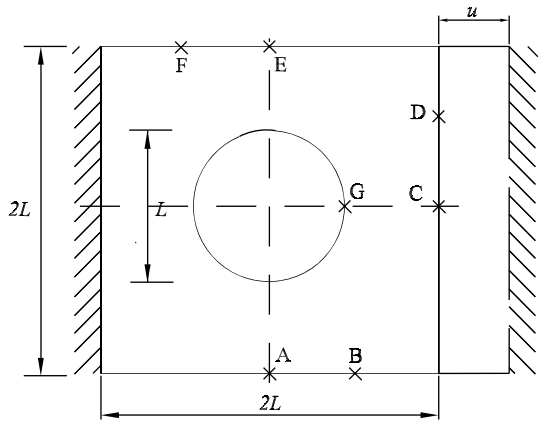

Fig. 4. Definition of points for comparison, loadcase 2.

Table 3
Comparison of displacements/tractions (whichever is free as boundary conditions) computed with an isotropic BEM code from Rus and Gallego (2002a,b) (a) and the present anisotropic BEM formulation (b)

Point	(a)		(b)		Error	
	x	y	x	y	x	y
A	0.5000	0.3096	0.5000	0.2745	0.00	3.51
B	0.6958	0.1785	0.6954	0.1464	0.04	3.21
C	0.0546	0.0000	0.0490	0.0000	0.56	0.00
D	0.3075	−0.0415	0.2776	−0.0365	2.99	0.50
E	0.5000	−0.3096	0.5000	−0.2757	0.00	3.39
F	0.3043	−0.1785	0.3051	−0.1468	0.08	3.17
G	0.9981	0.0000	0.9946	0.0001	0.35	0.01

Relative errors (%) with respect to the load $p = 1$.

numerical results of the measurements is performed, in order to establish the necessary compromise between computing time and precision. Fig. 5 shows how the values converge correctly as the number of elements and therefore the computing time grow.

5.2. Noise effects

The identifiability through analyzing the cost functional Ψ versus the parameter from incomplete data with unexpected random noises is first examined. If the cost functional approach any noticeable peak point, it is very easy to identify the defect. However, excessive noises could make deleterious contributions to the detection of the defect. The noise in the measurements is varied by using a Gaussian distribution with zero mean. The cost functional should give a maximum when it is close to the real position, which we set to: $x_1^{cg} = 0.10$, $x_2^{cg} = 0.20$, $a = 0.30$, $b = 0.20$, and $\alpha = 0.40$. The measurement data are the vertical component of the displacements at the uniformly spaced ten nodes in which the upper side of the square plate has been discretized by the BEM.

Fig. 6 shows the values of the cost function versus the rotation angle of the flaw for two composite materials, for increasing experimental noise. From Fig. 6 it may be noted that the glass-epoxy case gives somewhat better sensitivity, which we see from the fact that the cost function has a larger range of values and also that with 2–5% noise there is still possible to find a close value for the glass-epoxy model whereas it is

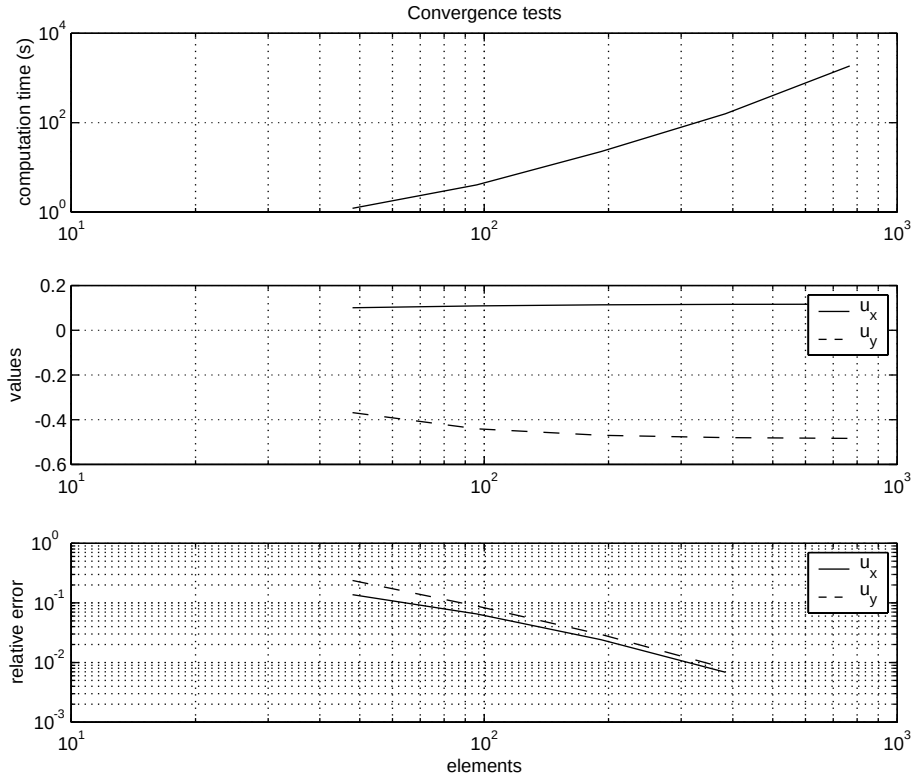

Fig. 5. Numerical convergence at measuring point A.

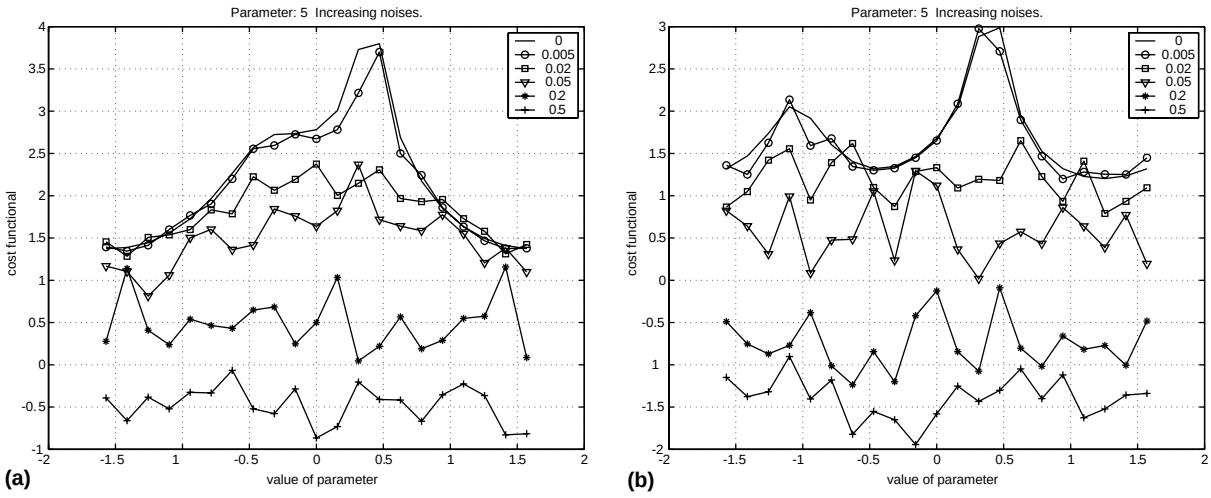

Fig. 6. Detection of rotaional angle (α) for different noise deffects (square model, load case 1, [45/0/0/45]): (a) glass-epoxy and (b) graphite-epoxy.

not possible in graphite-epoxy. A search algorithm is more likely to find that maximum simply because the maximum is noticeably higher than the neighbour values, and in this case the maximum is much closer to the real value, and more distinguishable. A very interesting observation in graphite-epoxy is that the fitness function shows a secondary maximum which means that there is a different angle that gives almost the same response as the original one, which may lead to a false guess of the absolute maximum for 2% noise. It is remarkable that in the glass-epoxy, a shallower second maximum tends to appear at a different position, varying from angle -0.3 radians to -1.1 in graphite-epoxy. It is important to take into account that the ellipse is not too flat, which makes the angle less identifiable (i.e. the overall geometry varies less when the defect rotates). Figs. 7 and 8 show the evolution of the identification cost function when the flaw is

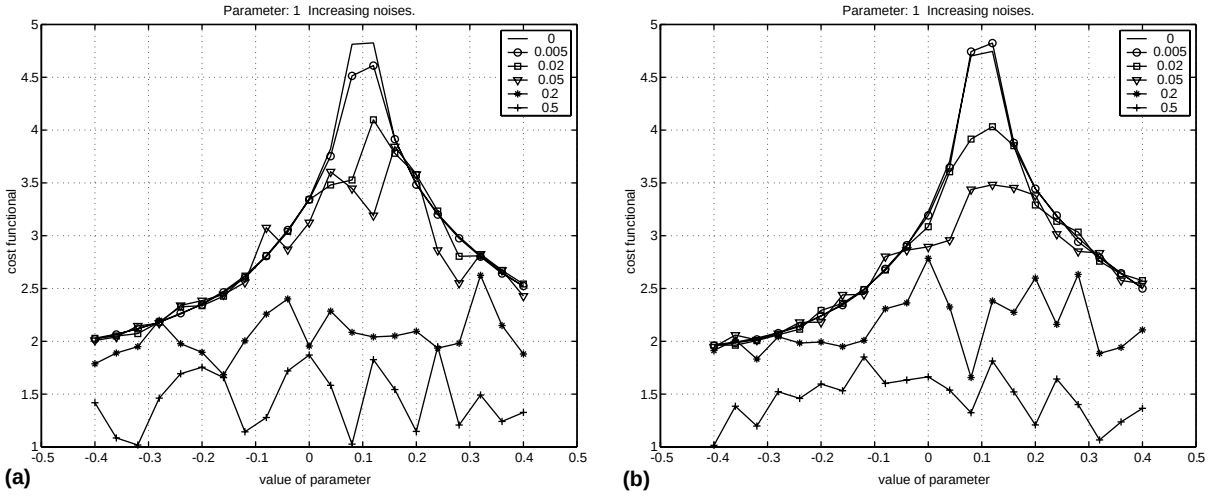

Fig. 7. Detection of horizontal coordiate (x_1^{cg}) for different noise effects (square model, load case 2, graphite-epoxy): (a) [45/0/0/45] and (b) [45/0/45].

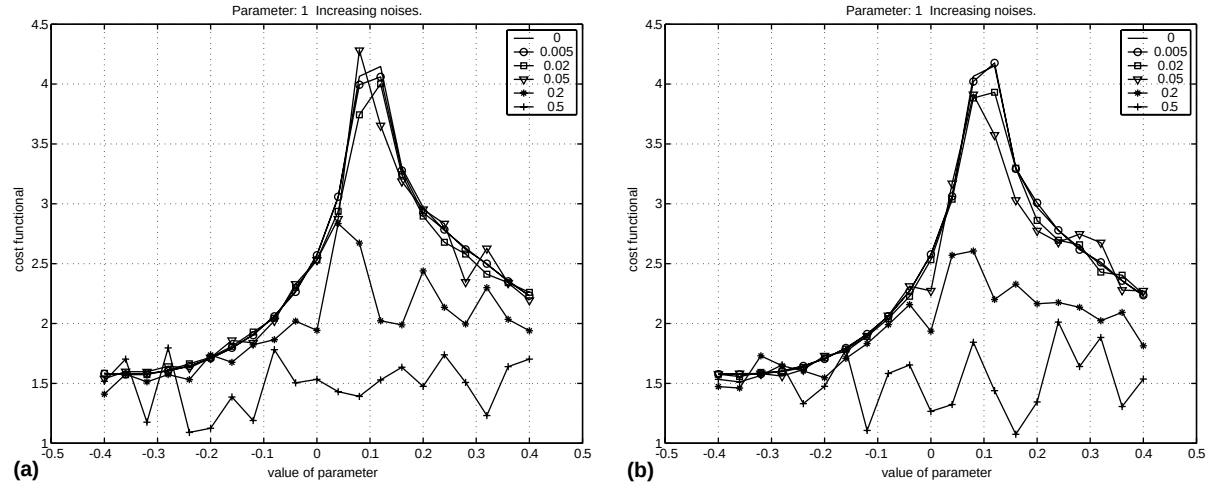

Fig. 8. Detection of horizontal coordiate (x_1^{cg}) for different noise effects (square model, load case 2, graphite-epoxy): (a) [45/0] and (b) [45].

moved horizontally in composites with four different symmetric angle-ply layups. It may be observed that the 1 and 2 layer setups are less sensitive to the noise.

A general observation about the non-convex nature of the inverse problem needs to be made. It can be observed already from the first figure that the convexity of the cost functional (in the sense of the positive semi-definiteness of its Hessian) is broken, as can be seen in the inflexion points and even multiple local extrema that grow with the level of noise and degree of material anisotropy.

5.3. Cross-ply

Fig. 9 shows the cost functional against the horizontal flaw size in cross-ply composites with different fiber angles. In combination with the load case, the results obtained without noises could be noticeably different depending on the given fiber angles. The models with fiber angles 30° and 45° are easy to examine in load case 1, whereas the 90°-model is very difficult. It is easy to understand that the lower levels of the cost function make it less capable to stand out above the noises. It may also be observed that load case 2 is less sensitive to the configuration of the fiber angles loadcase 1. Therefore, it is easier to identify because the cost function values are higher.

Fig. 10 studies the horizontal flaw size in cross-ply composites with different fiber angles. The used model is from now on the rectangular one (height=0.6L), where the real parameter values are $x_1^{cg} = 0.20$, $x_2^{cg} = 0.10$, $a = 0.10$, $b = 0.05$, and $\alpha = 0.40$, respectively. Fig. 10 presents the importance of the choice of the loadcase to find some parameters. Whereas load case 1 gives curves with low identifiability because of low cost function and especially a narrow peak, load case 2 is quite easy, especially for angles of 60, 45 and 90.

5.4. Angle-ply

Fig. 11 studies the horizontal flaw size in symmetric angle-ply composites using different number of layers. As shown in the figures, $[30/60]_s$ and [30/60/30] give the best identifiability, but not far ahead of the rest, excepting the $[30/0]_s$. The differences of the values in different fiber angles are slightly smaller in the case of three layers, although all very much at the same range of values. We may conclude from these results that the use of different layer sequences make little differences for the identification of the size.

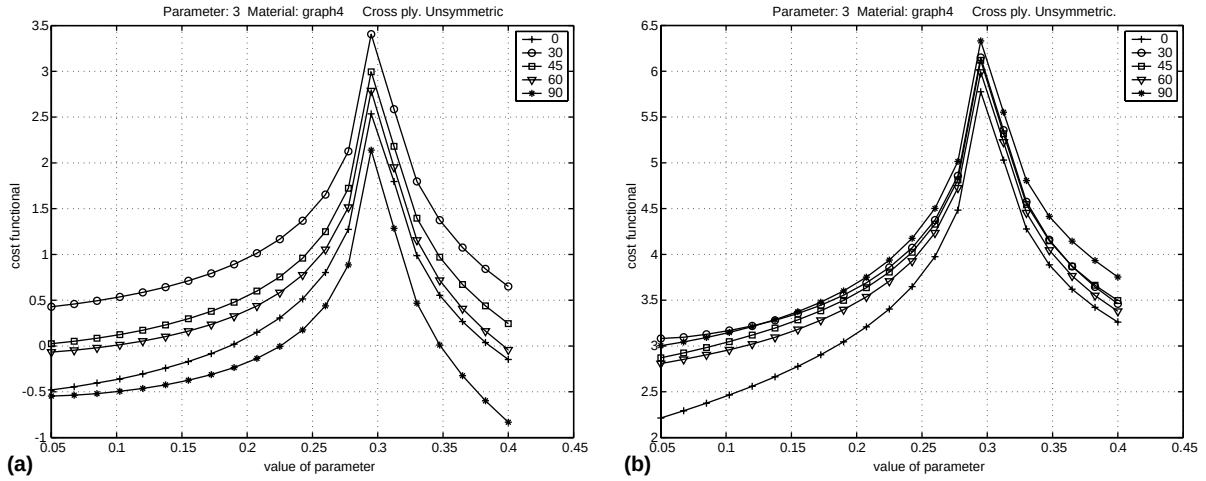

Fig. 9. Detection of horizontal size (a) for different fiber angles in noise free (square model, graphite-epoxy, $[\beta/\beta \pm 90/\beta/\beta \pm 90]$, $\beta = 0$–90): (a) loadcase 1 and (b) loadcase 2.

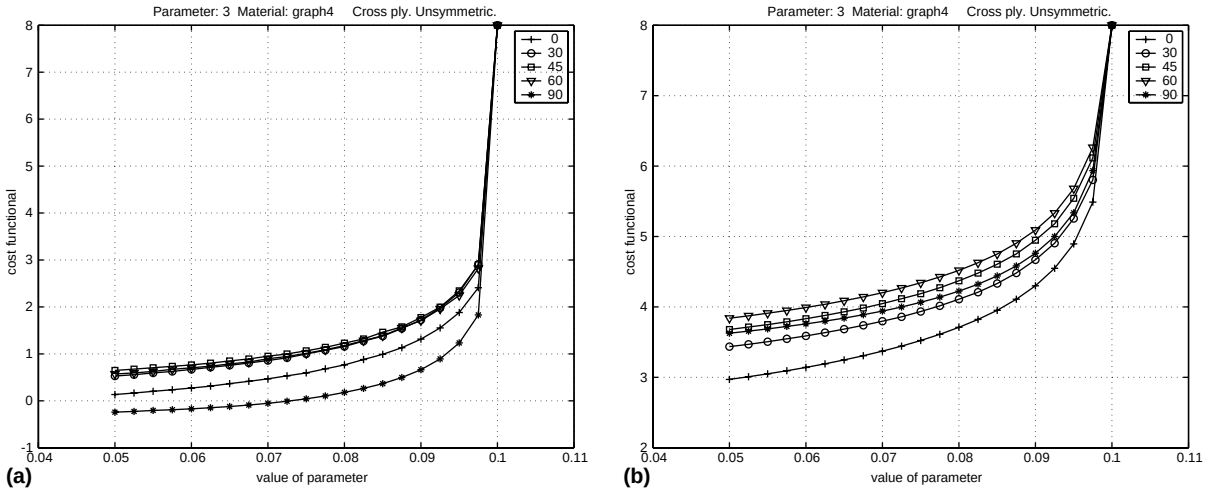

Fig. 10. Detection of horizontal size (a) for different fiber angles in noise free (rectangular model, graphite-epoxy, $[\beta/\beta \pm 90/\beta/\beta \pm 90]$, $\beta = 0$–90): (a) loadcase 1 and (b) loadcase 2.

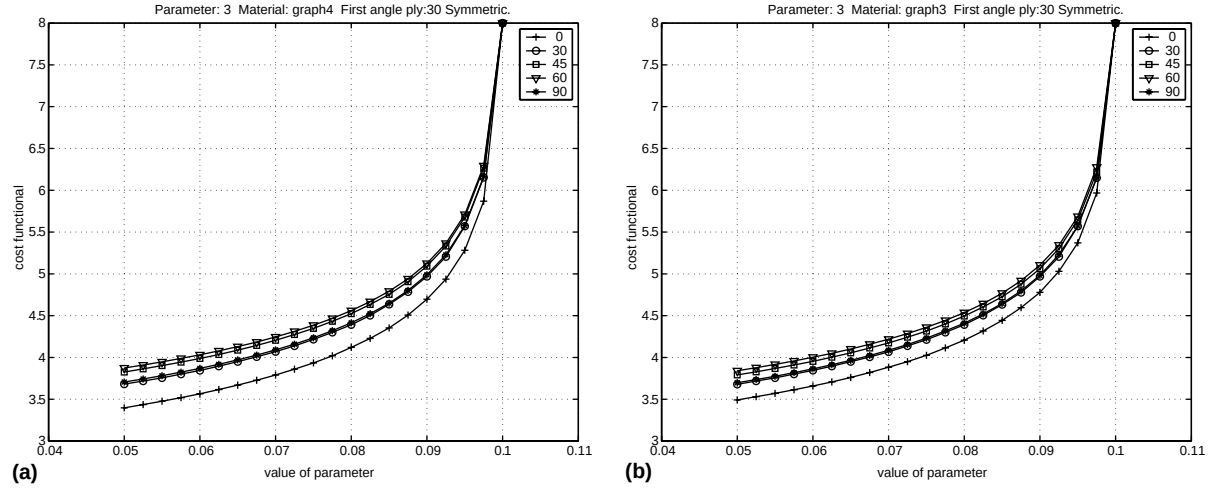

Fig. 11. Detection of horizontal size (a) for different fiber angles in noise free (rectangular model, graphite-epoxy, load case 2, $\beta =$ 0–90): (a) $[30/\beta/\beta/30]$ and (b) $[30/\beta/30]$.

Fig. 12 shows a similar case as above but for a different combination of angles. From the figure, [60/45] and [60/45/60] present the best identifiability as opposed to [60/0] and [60/0/60]. It may be also noted that the position of a secondary maximum ($\doteq -1.0 \sim -1.5$ radians) appears at different positions for different angles, which is closely related to the anisotropic nature of the composite materials.

5.5. Combination of parameters

In Fig. 13, we provide the perspectives for the variation of the cost functional with two parameters at the same time. It is noted that there are some correlations between the parameters (see that the horizontal

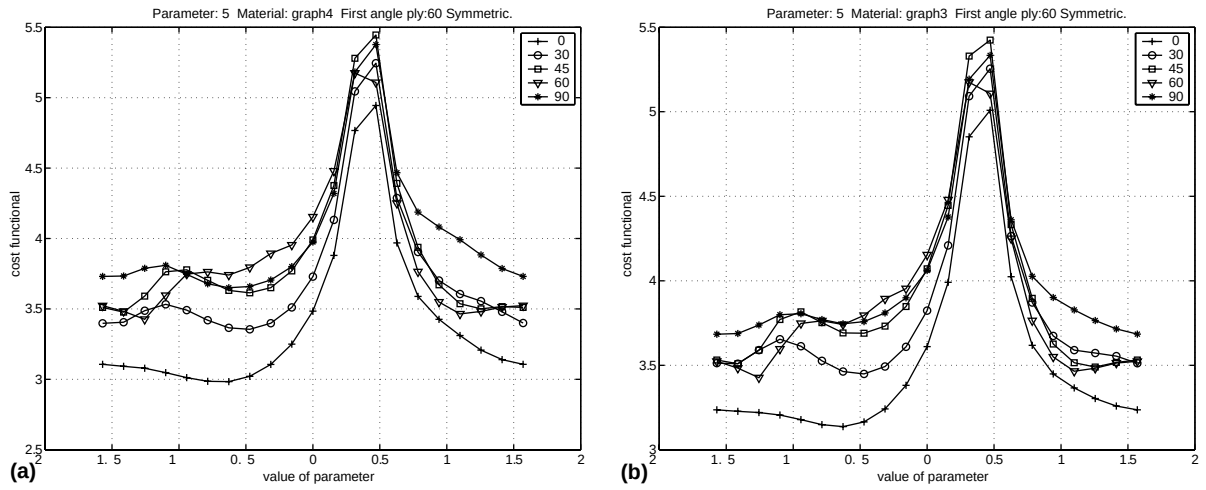

Fig. 12. Detection of horizontal size (a) for different fiber angles in noise free (rectangular model, graphite-epoxy, load case 2, $\beta = 0$–90): (a) [60/β/β/60] and (b) [60/β/60].

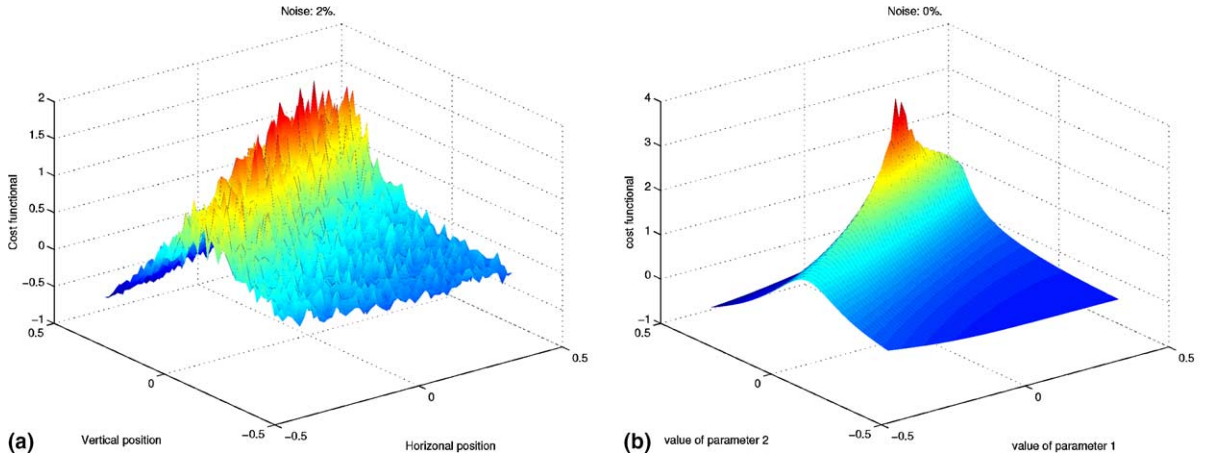

Fig. 13. Combination of horizontal and vertical coordinates (x_1^{cg} and x_2^{cg}, graphite-epoxy, four layers. Square model, load case 1): (a) noise 2% and (b) noise 0%.

section of the mountain-shaped surface is not circular, but very oblong) which makes it more difficult to find the exact position of the defect in that zone. It can be understood conversely that it is particularly easy to distinguish the location perpendicularly to that direction.

6. Summary and Conclusion

An inverse technique is developed to identify various properties of anisotropic composites by using concept of POD. For the numerical simulation of the problem, the boundary element technique has been used for the first time to assess the identifiability of defects in those composites and foresee the applicability of

the family of identification methods based on the minimization of measurement discrepancy. The boundary element method is an attractive approach, not only because it is computationally efficient and accurate but also because we can avoid the domain meshing that is mandatory in FEM. The technique is then implemented for anisotropic composites of various layup sequences to compare the results obtained from different noises and load cases. The results obtained from the boundary element formulation for isotropic structure are compared with the results available in the open literature and a good agreement is observed. In the numerical results, we observe that the use of different number of layers make little difference for detecting the sizes or positions regardless of fiber angles, but the difference becomes significant for the loading conditions and noise effects. It is also checked that the non-convex nature of the inverse problem is always present and magnified for stronger noise and material anisotropy.

The most relevant results to quantify the level of noise that limits the identifiability of defects in relationship with angle and fiber layup, loading conditions and defect position are shown in this work. Although no simple formula for the identifiability is found, the general theoretical conclusions have been tested quantitatively. The conclusions described in this paper are not restricted to the use of the boundary element method, but to any inversion strategy based on finding the defect characterizing parameters that minimize a cost functional in terms of discrepancy between computed and measured responses.

Acknowledgment

We would like to acknowledge the Fulbright Foundation and the Spanish Ministerio de Educación Culturay Deporte for the postdoctoral fellowship supporting this work.

References

Achenbach, J.D., 2000. Quantitative nondestructive evaluation. International Journal Solids and Structures 37, 13–27.

Aithal, R., Saigal, S., 1995. Shape sensitivity in thermal problems using BEM. Engineering Analysis with Boundary Elements 15, 115–120.

Bezerra, L.M., Saigal, S., 1993. A boundary element formulation for the inverse elastostatics problem (IESP) of flaw detection. Internal Journal of Numerical Methods in Engineering 36, 2189–2202.

Bonnet, M., 1995. Boundary integral equations and material differentiation applied to the formulation of obstacle inverse problems. Engineering Analysis with Boundary Elements 15, 121–136.

Bonnet, M., 1999. A general boundary-only formula for crack shape sensitivity of integral functionals. Comptes Rendus de l'Acadmie des Sciences 327 (12), 1215–1221.

Boström, A., Wirdelius, H., 1995. Ultrasonic probe modeling and nondestructive crack detection. Journal of the Acoustic Society of America 97, 2836–2848.

Burczyński, T., 1993. Recent advances in boundary element approach to design sensitivity analysis—a survey. In: Kleiber, M. (Ed.), Design Sensitivity Analysis, pp. 1–25.

Burczyński, T., Kane, J.H., Balakrishna, C., 1995. Shape design sensitivity analysis via material derivative—adjoint variable technique for 3-D and 2-D curved boundary elements. International Journal of Numerical Methods in Engineering 38, 2839–2866.

Calmon, P., Lhémery, A., Locoeur-Thaïbi, I., Raillon, R., Paradis, L., 1998. Models for the computation of ultrasonic fields and their interaction with defects in realistic NDT configurations. Nuclear Engineering and Design 180, 271–283.

Cruse, T.A., Swedlow, J.L., 1971. Interactive program for analysis and design problems in advanced composites technology. Report AFML-TR-71-268, Carnegie-Mellon University.

Domínguez, J., 1993. Boundary Elements in Dynamics. Elsevier, CMP.

Gallego, R., Rus, G., 2001. Sensitivity computation in elasticity with respect to shape, material properties and topology. In: Denda, M., Aliabadi, M.H., Charafi, A. (Eds.), Advances in Boundary Element Techniques.

Gallego, R., Suárez, J., 1999. Numerical solution of the variation boundary integral equation for inverse problems. International Journal of Numerical Methods in Engineering 49, 501–518.

Kane, J.H., Guru Prasad, K., 1993. Boundary formulations for sensitivity analysis without matrix derivatives. AIAA Journal 31 (9), 1731–1734.

Lee, S.Y., Wooh, S.C., in press. Waveform-based identification of structural damage using the combined FEM and microgenetic algorithms. Structural Engineering, ASCE.

Lee, S.Y., Yhim, S.S., Chang, S.Y., 1997. A study on the plane stress problem of composite laminated annular plates using finite difference method. Journal of KSSC 9-1, 65–79.

Lekhnitskii, S.G., 1981. Theory of Elasticity of an Anisotropic Body. MIR Publishers, Moscow.

Linderholt, A., Abrahamsson, T., 2003. Parameter identifiability in finite element model error localisation. Mechanical Systems and Signal Processing 17, 579–588.

Lingyun, P., Daniel, O.A., Frank, J.R., 1998. Boundary element analysis for composite materials and a library of Green's functions. Computers and Structures 66 (5), 685–693.

Mellings, S.C., Aliabadi, M.H., 1995. Flaw identification using the boundary element method. International Journal of Numerical Methods in Engineering 38, 399–419.

Nishimura, N., 1997. Crack determination problems. Theoretical and Applied Mechanics 46, 39–57.

Ogilvy, J.A., 1993. Model for predicting ultrasonic pulse-echo probability of detection. NDT & E International 26, 19–29.

Rajesh, S.N., Udpa, L., Udpa, S.S., 1992. Estimation of eddy current probability of detection (pod) using finite element method. Review of Progress in Quantitative Nondestructive Evaluation, La Joya, CA, USA, vol. 12B, pp. 2365–2372.

Rus, G., 2001. Numerical methods for nondestructive identification of defects. Ph.D. thesis, Universidad de Granada, E.T.S.I. Caminos, C.

Rus, G., Gallego, R., 2000. Solution of identification inverse problems by a sensitivity boundary integral equation, Barcelona, September, In: Suárez, B., Oñate, E., Bugeda, G. (Eds.), ECCOMAS2000.

Rus, G., Gallego, R., 2002a. Gradiente analítico para la identificación no destructiva de defectos mediante el método de los elementos de contorno. madrid, In: Abascal, R., Domínguez, J., Bugeda, G. (Eds.), CIMNE.

Rus, G., Gallego, R., 2002b. Optimization algorithms for identification inverse problems with the boundary element method. Engineering Analysis with Boundary Elements 26 (4), 315–327.

Snyder, M.D., Cruse, T.A., 1975. Boundary-integral equation analysis of cracked anisotropic plates. International Journal of Fracture 11 (2), 315–328.

Stavroulakis, G.E., 2001. Inverse and Crack Identification Problems in Engineering. Kluwer Academic Publishers.

Stavroulakis, G.E., Antes, H., 1998. Crack detection in elastostatics and elastodynamics. A BEM modelling—neural network approach. In: Tanaka, M., Dulikravich, G., (Eds.), Inverse Problems in Engineering Mechanics.

Suárez, F.J., 1998. Aplicacin del Mtodo de los Elementos de Contorno a la Resulucin del Problema Inverso en Elastodinmica. Ph.D. thesis, Universidad de Granada, E.T.S.I. Caminos.

Tanaka, M., Masuda, Y., 1989. Boundary element method applied to some potential inverse problems. Engineering Analysis 3 (3), 138–143.

Wang, C.Y., Achenbach, J.D., Hirose, S., 1996. Two-dimensional time domain BEM for scattering of elastic waves in solids of general anisotropy. International Journal of Solids and Structures 22 (26), 3843–3864.

Widagdo, D., Aliabadi, M.H., 2001. Boundary element analysis of cracked panels repaired by mechanically fastened composite patches. Engineering Analysis with Boundary Elements 25 (339), 45.

Wilson, R.B., Cruse, T.A., 1978. Efficient implementation of anisotropic three dimensional boundary integral equation analysis. International Journal of Numerical Method in Engeering 12 (9), 1383–1397.

Wirdelius, H., 1994. An optimization technique for inverse crack detection. Comm. Div. Mech. Div. of Mechanics, CTH, Göteborg, 11.

Yao, Z., Gong, B., 1994. Defect identification using boundary element methods of elastostatics. In: Tanaka, Bui et al. (Eds.), Inverse Problems in Engineering Mechanics.

Young, A., Rooke, D.P., Cartwright, D.J., 1992. Analysis of patched and stiffened cracked panels using the boundary element method. International Journal of Solids and Structures 29 (17), 2201–2216.